Supplemental Material

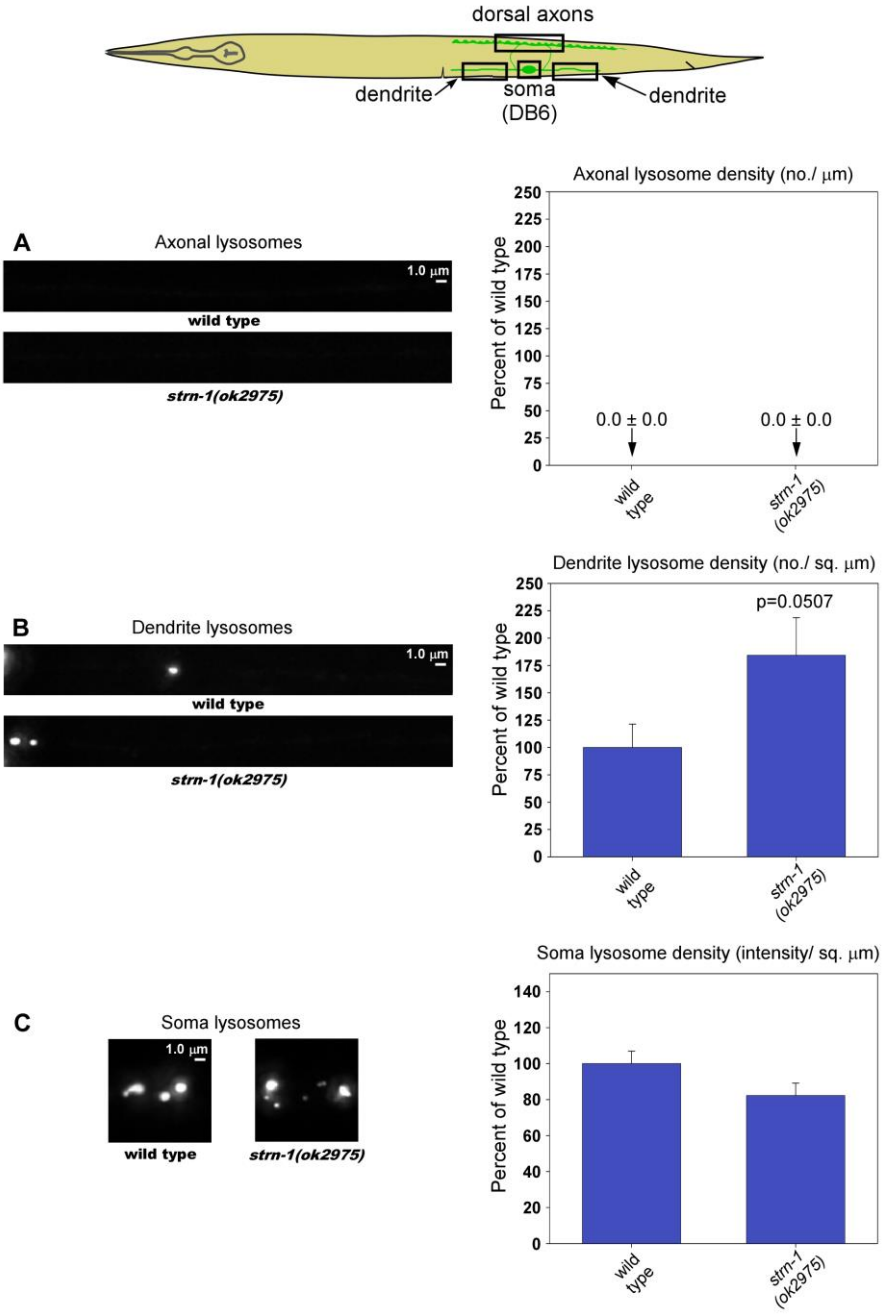

Figure S1. In the presence of JIP3, lysosomes have a wild type distribution in a *strn-1* null mutant (related to Figure 1).

Drawing illustrates location and anatomy of the cholinergic motor neurons imaged in this figure. Boxes outline the regions imaged. **(A- C)** Representative, identically-scaled images and quantification of lysosomal puncta and total fluorescence per micron in the dorsal axons **(A)**, ventral dendrites **(B)** and somas **(C)** of the indicated genotypes. Lysosomes are marked with CTNS-1-RFP, which is expressed from the integrated transgene *ceIs56*. Data are means and SEMs from 12-13 animals per region.

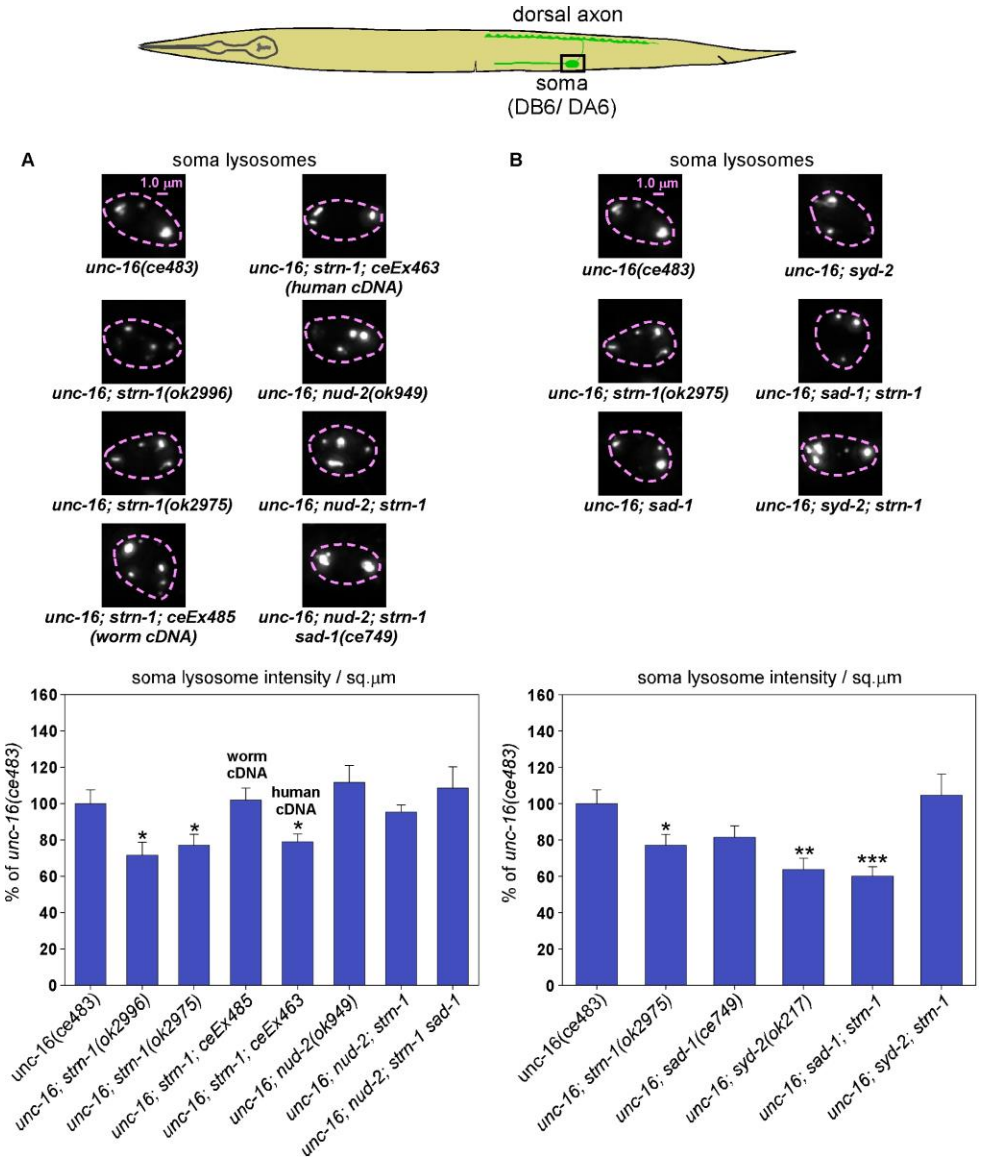

Figure S2. In an *unc-16(-)* background, *strn-1* null mutations are associated with a significant dynein-dependent depletion of lysosome density in cell somas (related to Figure 1 and Figure 2).

(A-B) Rectangle in drawing indicates region imaged. Representative, identically-scaled images and quantification of lysosome intensity per square micron in DB6/ DA6 somas in the indicated genotypes. The lysosome marker CTNS-1-RFP is expressed from the integrated transgene *ceIs56*. Graph data are means and standard errors of lysosome intensity per square micron from 13-18 animals each. Unmarked bars are not significantly different from *unc-16(ce483)*. *, **, and *** indicate P-values that are <.05, <.01, or <.001, respectively. Asterisks compare the indicated bar to *unc-16(ce483).*

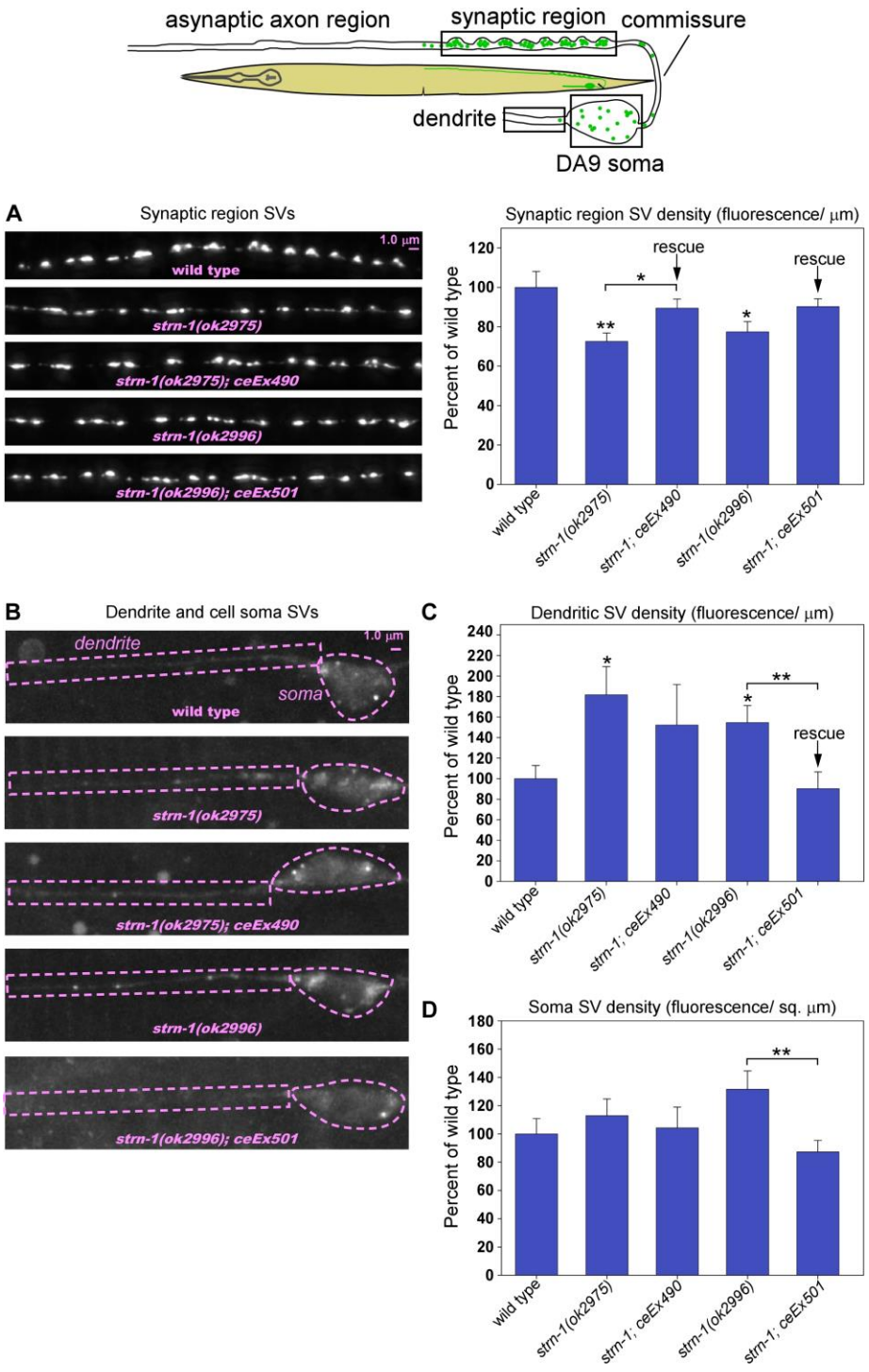

Figure S3. Sentryn acts cell-autonomously in DA9 to optimize the transport of SVs to clusters and to keep SVs out of dendrites (related to Figure 4).

(A-D) Rectangles in the drawing indicate regions imaged. Representative images and quantification of SV density in the indicated regions of the DA9 cholinergic motor neuron in the indicated genotypes. The SV marker GFP-RAB-3 is expressed from the integrated transgene *wyIs85*. Representative images are identically-scaled for each region. Dashed lines outline the dendrite and soma regions. Graph data are means and standard errors from 12-16 animals each. Unmarked bars are not significantly different from wild type. * and ** indicate P-values that are <.05 or <.01, respectively. Asterisks that are not above relationship bars compare the indicated bar to wild type.

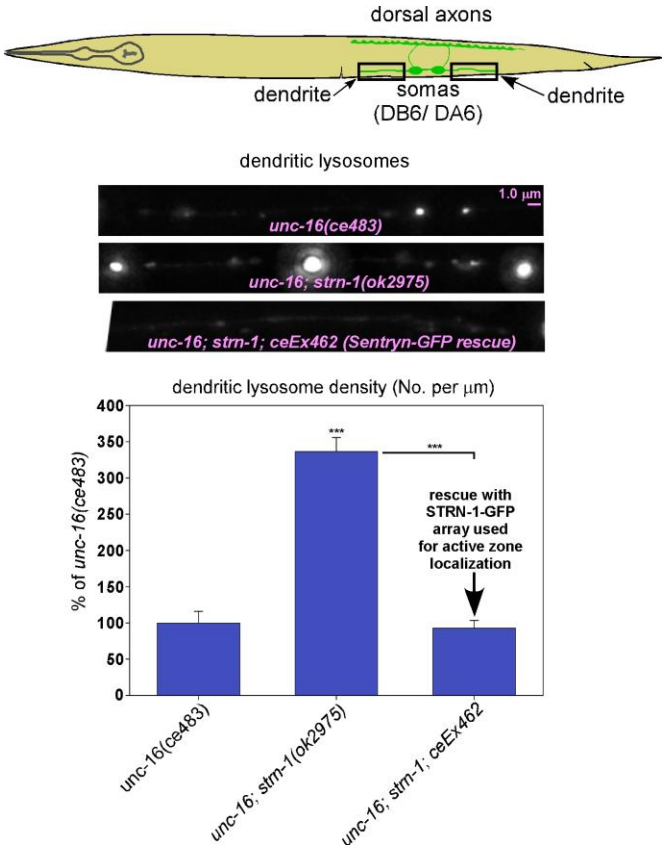

Figure S4. Demonstration that the Sentryn-GFP transgene used for active zone imaging restores wild type function to a Sentryn null mutant (related to Figure 9).

Rectangles in drawing indicate regions imaged. Representative, identically-scaled images of lysosome intensity in DB6/ DA6 somas in the indicated genotypes. The lysosome marker CTNS-1-RFP is expressed from the integrated transgene *ceIs56*. The *ceEx462* extrachromosomal array expresses STRN-1-GFP in a subset of DA/ DB cholinergic motor neurons. The plasmid expressing strn-1-GFP was injected at the low level of 700 picograms/ µl to ensure that STRN-1-GFP is not over-expressed. Graph data are means and standard errors from 15 animals each. Unmarked bars are not significantly different from wild type. *** indicate P-values that are <.001. Asterisks that are not above relationship bars compare the indicated bar to wild type.

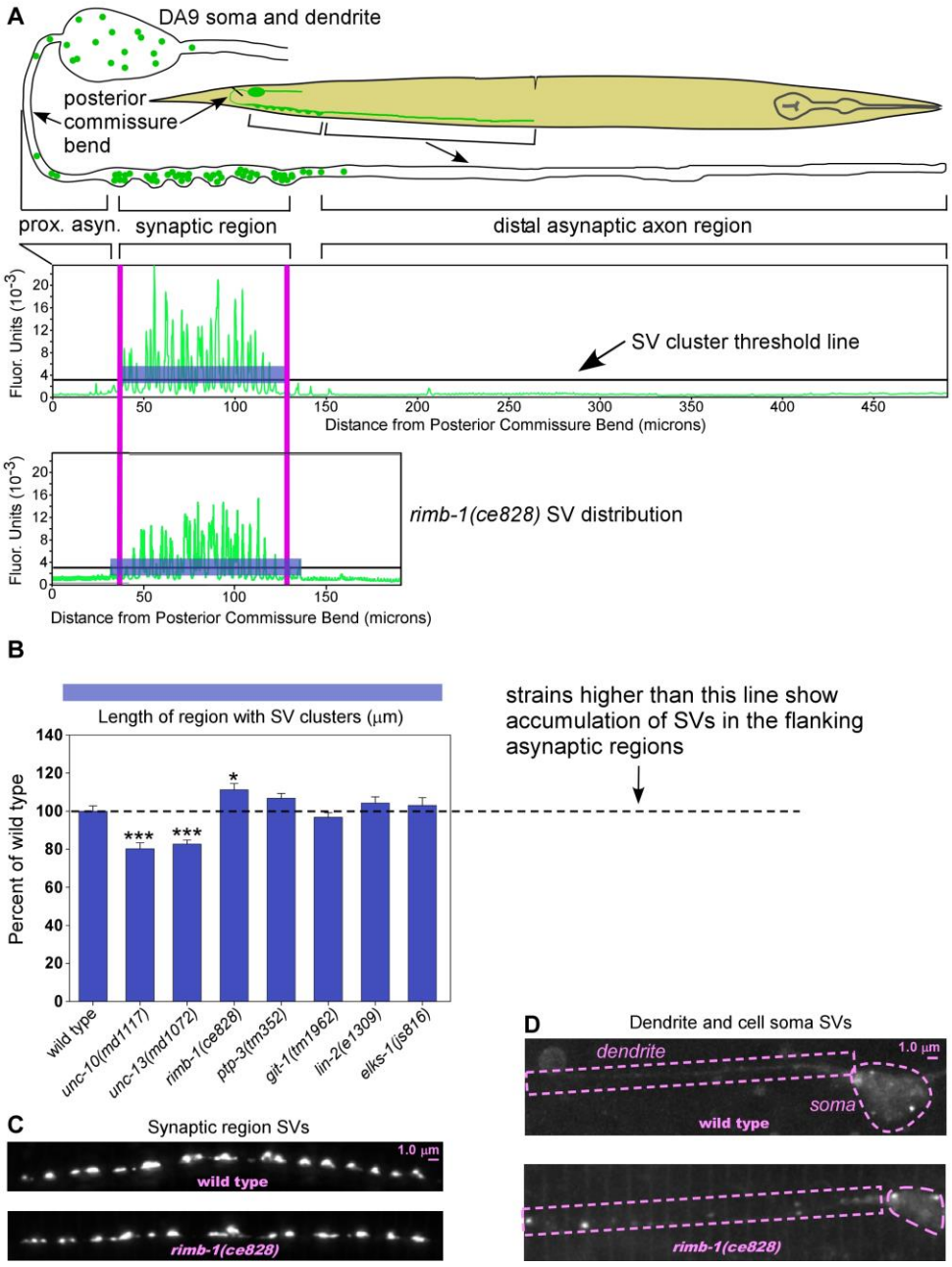

Figure S5. Null mutations in most non-CSS active zone-enriched proteins do not impair SV capture.

(A) Drawing indicates regions of the DA9 motor neuron. Graphs plot fluorescence intensity of the SV marker GFP-RAB-3 as a function of distance from the posterior commissure bend for a single representative animal of each indicated genotype. A threshold line indicates the intensity cut-off used for defining SV clusters. Blue highlighted segments indicate regions exceeding the threshold in wild type and a *rimb-1* null mutant. High resolution images acquired with a large field-of-view Flash 4.0 camera were used to reconstruct the dorsal axon from multiple images. GFP-RAB-3 is expressed from the integrated transgene array *wyIs85*.

(B) Graph quantifies SV capture efficiency in the indicated genotypes by measuring the length of the region with SV clusters exceeding the threshold line (shown in (A)). This quantifies the extent to which SVs have overshot the synaptic region and have moved toward microtubule plus ends in the long asynaptic region. Graph data are means and standard errors from 14-15 animals each. Unmarked bars are not significantly different from wild type. * and *** indicate P-values that are <.05 or <.001, respectively, and compare the indicated bar to wild type. The *C. elegans* gene names and the common names of each protein are as follows, along with one or more references demonstrating that the protein is enriched at active zones: UNC-10 (RIM: Rab3 Interacting Molecule) (Koushika et al., 2001; Wang et al., 1997), UNC-13 (Charlie et al., 2006a; Weimer et al., 2006); RIMB-1 (RIM-Binding Protein) (Liu et al., 2011; Wang et al., 2000), PTP-3 (LAR: Leukocyte-common Antigen Related) (Ackley et al., 2005), GIT-1 (GIT: G protein coupled receptor kinase 2 Interacting protein) (Kim et al., 2003), LIN-2 (CASK: name ontology unknown) (Olsen et al., 2005), ELKS-1 (ELKS/ ERC/ Bruchpilot) (Deken et al., 2005; Kittel et al., 2006; Ohtsuka et al., 2002; Wagh et al., 2006; Wang et al., 2002). Evidence that 5 of these active zone enriched proteins interact with SYD-2 (Liprin-α) in *C. elegans* or other animals is as follows: in *C. elegans* and/ or other animals: ELKS (Dai et al., 2006; Kittelmann et al., 2013; Ko et al., 2003b), RIM (Schoch et al., 2002), CASK (Olsen et al., 2005), LAR (Serra-Pages et al., 1998), and GIT (Ko et al., 2003a).

(C, D) Representative images of SV density in the indicated regions of the DA9 cholinergic motor neuron in the indicated genotypes. The SV marker GFP-RAB-3 is expressed from the integrated transgene *wyIs85*. Representative images are identically-scaled for each region. Dashed lines outline the dendrite and soma regions. See text for quantifications associated with the image sets from which these representative images were taken.

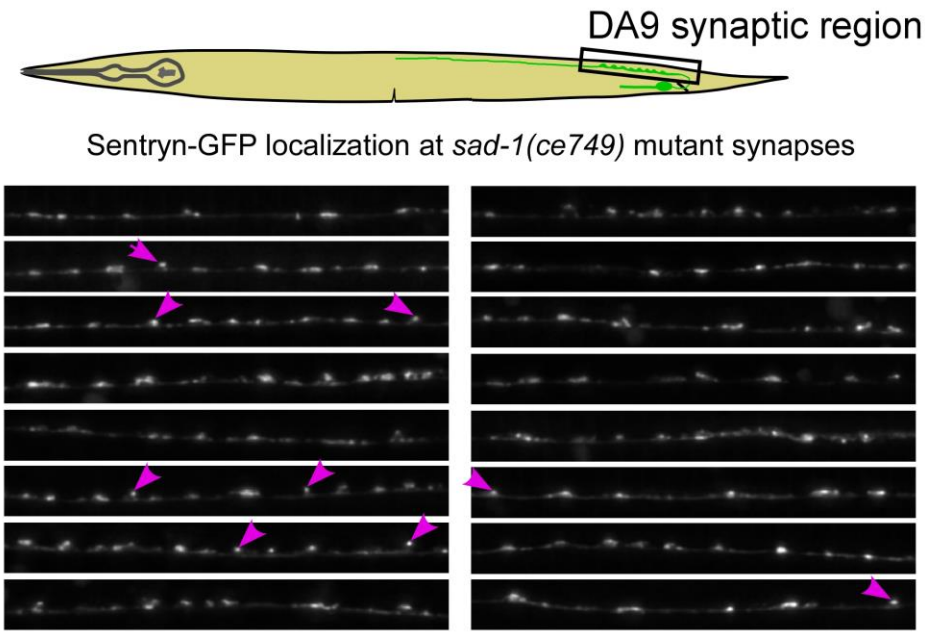

Figure S6. Sentryn shows variable localization in synaptic bouton lacking SAD Kinase (related to Figure 9).

Rectangle in drawing shows region imaged. Panel of images from different animals showing localization of Sentryn-GFP in the synaptic region in the indicated mutant backgrounds. Note that Sentryn localization appears partially disrupted, sometimes localizing to the ventral apex (pink arrowheads) and sometimes appearing unlocalized or localizing to bouton regions other than the ventral apex. Readers are encouraged to use on-screen magnification and to compare to the image from wild type in Figure 9B. Sentryn-GFP is expressed from the *ceEx462* transgenic array.

Table S1. *C. elegans* non-wild type Strains.

Strain name	Genotype (origin and/ or first use cited if not produced in this study)
KG4790	*ceEx462 [unc-129::STRN-1-GFP]*
KG5131	*ceEx503 [mig-13::UNC-10-GFP, Td Tomato-STRN-1]*
KG5203	*ceEx510 [mig-13::STRN-1-Emerald, SAD-1-tdTomato]*
KG2882	*ceIs123 [unc-129::GFP, ttx-3::mCherry]* (Hoover, 2014)
KG4671	*ceIs259 [unc-129::RFP-SYN-13, -Venus]* (Edwards, 2015)
KG2430	*ceIs56 [unc-129::CTNS-1-RFP, unc-129::nlp-21-Venus]* (Edwards, 2009)
KG4846	*elks-1(js816); wyIs85 [itr-1::GFP-RAB-3, odr-1::RFP]*
KG5030	*git-1(tm1962); wyIs85 [itr-1::GFP-RAB-3, odr-1::RFP]*
KG5011	*lin-2(e1309); wyIs85 [itr-1::GFP-RAB-3, odr-1::RFP]*
KG4506	*nud-2(ok949); wyIs85 [itr-1::GFP-RAB-3, odr-1::RFP]*
KG5021	*ptp-3(tm352); wyIs85 [itr-1::GFP-RAB-3, odr-1::RFP]*
KG5029	*rimb-1(ce828); wyIs85 [itr-1::GFP-RAB-3, odr-1::RFP]*
KG4400	*sad-1(ce749) [2X o.c.]*
KG4822	*sad-1(ce749); ceEx462 [unc-129::STRN-1-GFP]*
KG4941	*sad-1(ce749); ceIs123 [unc-129::GFP, ttx-3::mCherry]*
KG4610	*sad-1(ce749); wyIs85 [itr-1::GFP-RAB-3, odr-1::RFP]*
KG4932	*strn-1(ok2975) [4x O.C.]*
KG4740	*strn-1(ok2975) ceIs56 [unc-129::CTNS-1-RFP, unc-129::nlp-21-Venus]*
KG4833	*strn-1(ok2975) sad-1(ce749)*
KG4945	*strn-1(ok2975) sad-1(ce749); ceIs123 [unc-129::GFP, ttx-3::mCherry]*
KG4849	*strn-1(ok2975) sad-1(ce749); wyIs85 [itr-1::GFP-RAB-3, odr-1::RFP]*
KG5013	*strn-1(ok2975) syd-2(ok217) sad-1(ce749); wyIs85 [itr-1::GFP-RAB-3, odr-1::RFP]*
KG4812	*strn-1(ok2975) syd-2(ok217); wyIs85 [itr-1::GFP-RAB-3, odr-1::RFP]*
KG4887	*strn-1(ok2975); ceIs123 [unc-129::GFP, ttx-3::mCherry]*
KG4886	*strn-1(ok2975); ceIs259 [unc-129::RFP-SYN-13, -Venus]*
KG4787	*strn-1(ok2975); wyIs85 [itr-1::GFP-RAB-3, odr-1::RFP]*
KG4992	*strn-1(ok2975); wyIs85 [itr-1::GFP-RAB-3, odr-1::RFP]; ceEx490 [itr-1::STRN-1 cDNA]*
KG4490	*strn-1(ok2996) [4x O.C.]*
KG4933	*strn-1(ok2996) sad-1(ce749)*
KG4943	*strn-1(ok2996); wyIs85 [itr-1::GFP-RAB-3, odr-1::RFP]*
KG5126	*strn-1(ok2996); wyIs85 [itr-1::GFP-RAB-3, odr-1::RFP]; ceEx501 [itr-1::STRN-1 cDNA]*
KG4987	*syd-2(ok217) sad-1(ce749); wyIs85 [itr-1::GFP-RAB-3, odr-1::RFP]*
KG4821	*syd-2(ok217); ceEx462 [unc-129::STRN-1-GFP]*
KG4526	*syd-2(ok217); wyIs85 [itr-1::GFP-RAB-3, odr-1::RFP]*
KG4981	*unc-10(md1117); wyIs85 [itr-1::GFP-RAB-3, odr-1::RFP]*
KG5001	*unc-13(md1072); wyIs85 [itr-1::GFP-RAB-3, odr-1::RFP]*
KG4673	*unc-16(ce483); ceIs259 [unc-129::RFP-SYN-13, -Venus]*
KG4192	*unc-16(ce483); ceIs56 [unc-129::CTNS-1-RFP, unc-129::nlp-21-Venus]*
KG4573	*unc-16(ce483); nud-2(ok949); ceIs56 [unc-129::CTNS-1-RFP, unc-129::nlp-21-Venus]*
KG4931	*unc-16(ce483); nud-2(ok949); sad-1(ce749) strn-1(ok2975) ceIs56 [unc-129::CTNS-1-RFP, unc-129::nlp-21-Venus]*
KG4892	*unc-16(ce483); nud-2(ok949); strn-1(ok2975) ceIs56 [unc-129::CTNS-1-RFP, unc-129::nlp-21-Venus]*
KG4893	*unc-16(ce483); nud-2(ok949); syd-2(ok217) strn-1(ok2975) ceIs56 [unc-129::CTNS-1-RFP, unc-129::nlp-21-Venus]*
KG4498	*unc-16(ce483); sad-1(ce749) ceIs56 [unc-129::CTNS-1-RFP, unc-129::nlp-21-Venus]*
KG4811	*unc-16(ce483); sad-1(ce749) strn-1(ok2975) ceIs56 [unc-129::CTNS-1-RFP, unc-129::nlp-21-Venus]*
KG4750	*unc-16(ce483); strn-1(ok2975) ceIs56 [unc-129::CTNS-1-RFP, unc-129::nlp-21-Venus]*
KG4805	*unc-16(ce483); strn-1(ok2975) ceIs56 [unc-129::CTNS-1-RFP, unc-129::nlp-21-Venus]; ceEx463 [unc-129::STRN-1-Hs]*
KG4958	*unc-16(ce483); strn-1(ok2975) ceIs56 [unc-129::CTNS-1-RFP, unc-129::nlp-21-Venus]; ceEx485 [unc-129::STRN-1]*
KG4791	*unc-16(ce483); strn-1(ok2975) ceIs56; ceEx462 [unc-129::STRN-1—GFP]*
KG4905	*unc-16(ce483); strn-1(ok2975); ceIs259 [unc-129::RFP-SYN-13, -Venus]*
KG4520	*unc-16(ce483); strn-1(ok2996) ceIs56 [unc-129::CTNS-1-RFP, unc-129::nlp-21-Venus]*
KG4563	*unc-16(ce483); syd-2(ok217) ceIs56 [unc-129::CTNS-1-RFP, unc-129::nlp-21-Venus]*
KG4814	*unc-16(ce483); syd-2(ok217) strn-1(ok2975) ceIs56 [unc-129::CTNS-1-RFP, unc-129::nlp-21-Venus]*
TV1229	*wyIs85 [itr-1::GFP-RAB-3, odr-1::RFP]* (Klassen and Shen, 2007)

Table S2. Mutation lesions and methods used for genotyping in strain constructions.

Mutation	Description of Molecular Lesion	Effect on Protein	Method(s) used for genotyping	References
elks-1(js816)	494 bp deletion within exon 6. Splicing of remaining exon creates a frameshift that results in a stop codon at amino acid 292 (out of 837 amino acids).	Putative null	PCR with primers inside deleted region	(Deken et al., 2005)
git-1(tm1962)	483 bp deletion and 23 bp insertion beginning in intron 7, including all of exons 8 and 9, and ending in intron 9. Splicing of exon 7 to exon 10 creates a frameshift that results in a stop at amino acid 318 (out of 670 amino acids).	Putative null	PCR with primers inside deleted region	Japanese National Bioresource Project for the Experimental Animal "Nematode *C. elegans*" and (Patel et al., 2006)
lin-2(e1309)	Not published.	Putative null	Vulvaless and Egl-D phenotypes	(Ferguson and Horvitz, 1985)
nud-2(ok949)	1109 bp deletion and a 1 bp insertion. Starts at the predicted ATG of nud-2 and deletes the entire open reading frame except the last part of the last exon.	Putative null	PCR with primers inside deleted region	*C. elegans* Gene Knockout Consortium and (Fridolfsson et al., 2010)
ptp-3(tm352)	506 bp deletion in ptp-3a (bp# 1462-1967). Mutation eliminates exons 8 and 9. The subsequent splicing of exons 7 and 10 creates a frameshift at AA355 that results in a stop at AA357. This changes/eliminates 83.7% of the total protein.		PCR with primers inside deleted region	Japanese National Bioresource Project for the Experimental Animal "Nematode *C. elegans*" and (Ackley et al., 2005)
rimb-1(ce828)	13 bp insertion after AA16 (out of 1276 AA total) introduced through oligo templated Cas9 homologous recombination. Insert contains 3 stop codons, each in a different reading frame as well as an Nhe I site for screening.	Putative null	Make 542 bp PCR product centered on the insertion, followed by restriction digest with Nhe I (the insertion creates an Nhe I site). Confirm using PCR followed by sequencing.	This study
sad-1(ce749)	Q57Stop (out of 835 or 914 amino acids, depending on the isoform). Mutation position is the same in both isoforms.	Putative null	Make 250 bp PCR product centered on the mutation, followed by restriction digest with Mse I (the mutation creates an Mse I site).	(Edwards et al., 2015a)
strn-1(ok2975)	558 bp deletion and 49 bp insertion that causes a frameshift resulting in R178Stop (out of 457 amino acids). Changes/ eliminates approximately 72.5% of the protein.		PCR with primers inside deleted region	*C. elegans* Gene Knockout Consortium
strn-1(ok2996)	699 bp deletion with single bp (A) insertion. A97D and amino acids 98-222 (out of 457) are deleted; then the same reading frame resumes. Affects approximately 27.5% of the protein.		PCR with primers inside deleted region	*C. elegans* Gene Knockout Consortium
syd-2(ok217)	~2 Kb deletion covering most of the N-terminal coiled coil domains. Results in a frame shift and stop codon at amino acid 200 (out of 1139 amino acids total).	Putative null	Behavioral phenotypes and PCR with primers inside deleted region	*C. elegans* Gene Knockout Consortium and (Kittelmann et al., 2013; Wagner et al., 2009)
unc-10(md1117)	Deletion of entire unc-10 coding region.	Null	PCR with primers inside deleted region	(Koushika et al., 2001)
unc-13(md1072)	26- to 38-kb deletion that eliminates all of the L coding region		Behavioral phenotypes and PCR with primers inside deleted region	(Kohn et al., 2000)

unc-16(ce483)	Q304Stop (out of1157 amino acids of the ZK1098.10b isoform)	Putative null	Behavioral phenotypes and PCR followed by sequencing	(Edwards et al., 2013)

Table S3. Transgenic and Integrated arrays.

Array name	**Insertion location in genome**	**Experimental contents and injection concentrations**	**Co-transformation markers and injection concentrations**	**References for transgene or integrated insertion (if not made in this study)**
ceEx462	extrachromosomal array	KG#797 (unc-129::STRN-1-GFP) (0.7 ng/ μl)	KG#67 (ttx-3::GFP) (25 ng/ μl)	this study
ceEx463	extrachromosomal array	KG#799 (unc-129::STRN-1-Hs cDNA) (5 ng/ μl)	KG#67 (ttx-3::GFP) (25 ng/ μl)	this study
ceEx485	extrachromosomal array	KG#818 (unc-129::STRN-1 cDNA) (2.5 ng/ μl)	KG#67 (ttx-3::GFP) (25 ng/ μl)	this study
ceEx490	extrachromosomal array	KG#819 (itr-1::STRN-1) (1 ng/ μl)	KS#5 (odr-1::GFP) (20 ng/ μl)	this study
ceEx501	extrachromosomal array	KG#819 (itr-1::STRN-1 cDNA) (4 ng/ μl)	KS#5 (odr-1::GFP) (20 ng/ μl)	this study
ceEx503	extrachromosomal array	KG#840 (mig-13::UNC-10 [627-974]-GFP) (1.5 ng/ μl) KG#899 (mig-13::tdTomato-STRN-1) (1.5 ng/μl)	KS#4 (odr-1::RFP) (20 ng/ μl)	this study
ceEx510	extrachromosomal array	KG#917 (mig-13::STRN-1-Emerald) (1.0 ng/ μl) KG#921 (mig-13::SAD-1-tdTomato) (1.0 ng/ μl)	KS#4 (odr-1::RFP) (20 ng/ μl)	this study
ceIs123	I: ~13.31	KG#367 [unc-129::GFP] (5 ng/ μl)	KG#255 [ttx-3::RFP] (25 ng/ μl)	(Hoover et al., 2014)
ceIs259	IV: ~3.4	KG#414 [unc-129::RFP-SYN-13] (1.0 ng/ μl) KG#374 [unc-129::mCherry] (1.0 ng/ μl)	KG#255 (ttx-3::RFP) (15 ng/ μl)	this study
ceIs56	X: ~9.0	KG#371 [unc-129::CTNS-1a-RFP] (5 ng/ μl)	KG#255 [ttx-3::RFP] (15 ng/ μl) KP#1383 unc-129::NLP-21-Venus (15 ng/ μl)	(Edwards et al., 2009; Edwards et al., 2013)
wyIs85	V: near 4.63	itr-1::GFP-RAB-3 – 10 ng/ μl	odr-1::dsRed - 20 ng/ μl	(Klassen and Shen, 2007)

Table S4. Plasmids.

Plasmid name	Brief Description	Cloning details or reference giving cloning details
KG#67	ttx-3::GFP	Gift of Oliver Hobert, Columbia University
KG#230	unc-129:: expression vector	(Edwards et al., 2009)
KG#255	ttx-3::RFP	(Edwards et al., 2009)
KG#367	unc-129:___-GFP	(Edwards et al., 2013)
KG#371	unc-129::ctns-1a-RFP (mCherry)	(Edwards et al., 2013)
KG#374	unc-129::___-Venus expression vector	(Edwards et al., 2009)
KG#414	unc-129::RFP-SYN-13	(Edwards et al., 2013)
KG#471	mig-13:: expression vector	(Edwards et al., 2015b)
KG#473	mig-13::___-GFP	Used Kpn I/ Apa I to cut out the ~1000 bp unc-54 3' control region from KG#471, leaving the 6.0 kb vector fragment containing the mig-13 promoter. To this vector fragment, we will ligate the 1800 bp Kpn I/ Apa I fragment (containing GFP + unc-54 3' control region) cut from pPD94.81.
KG#695	unc-129::SAD-1-GFP cDNA	(Edwards et al., 2015b)
KG#720	rab-3::STRN-1-FLAG cDNA	Used AffinityScript Multiple Temperature Reverse Transcriptase and a primer engineered with a restriction site and FLAG tag to make the strn-1-FLAG cDNA (1470 bp). Used Herculase II polymerase and primers engineered with restriction sites to amplify and clone the cDNA into Nhe I/ Kpn I cut KG#59 (rab-3::___ expression vector; 4.9 Kb).
KG#730	itr-1::expression vector	(Edwards et al., 2015b)
KG#797	unc-129::STRN-1-GFP	Used Herculase II DNA polymerase and primers engineered with restriction sites to amplify and clone the 1.4 Kb strn-1 (C16E9.2) cDNA (minus its stop codon) from KG#720 rab-3::strn-1-FLAG into Nhe I/ Kpn I cut KG#367 (unc-129::___-GFP; 7.2 Kb) such that it is in-frame with the GFP.
KG#799	unc-129::STRN-1-Hs (Homo sapiens)	Used Herculase II DNA polymerase and primers engineered with restriction sites to amplify and clone the 1.2 Kb strn-1-Hs cDNA (conserved protein KIAA0390) from the Genscript ORF clone ID OHu03925 into Nhe I/ Kpn I cut KG#230 (unc-129::___; 6.4 Kb).
KG#818	unc-129::STRN-1cDNA	Used Herculase II DNA polymerase and primers engineered with restriction sites to amplify and clone the 1470 bp strn-1 cDNA from KG#720 rab-3::strn-1-FLAG cDNA into Nhe I/ Kpn I cut KG#230 (unc-129::___; 6.4 Kb).
KG#819	itr-1::STRN-1cDNA	Used Herculase II DNA polymerase and primers engineered with restriction sites to amplify and clone the 1470 bp strn-1 cDNA from KG#720 rab-3::strn-1-FLAG cDNA into Nhe I/ Kpn I cut KG#730 (itr-1::___; 6.0 Kb).
KG#840	mig-13::UNC-10 [627-974]-GFP cDNA	Used AffinityScript Multiple Temperature Reverse Transcriptase and a primer engineered with a restriction site to make the unc-10 first strand cDNA starting at codon 974. Then used Herculase II polymerase and primers engineered with restriction sites and an artificial Met start codon to amplify and clone the 1044 bp UNC-10 [H627-R974] cDNA into Sbf I/ Kpn I cut KG#473 (mig-13::___GFP expression vector; 7.8 Kb).
KG#859	mig-13::INS-22-Emerald	Used ApE to digitally construct the plasmid, then design the primers necessary to assemble INS-22-Emerald in the mig-13:: vector background. Then used Q5 Polymerase to produce the fragments and the NEBuilder Master Mix to make the new plasmid.
KG#899	mig-13::tdTomato--STRN-1	Used ApE to digitally construct the plasmid, then designed the primers necessary to assemble tdTomato + a 2XGGSG linker onto the N-terminus of the strn-1 cDNA (PCRed from KG#818 unc-129::strn-1 cDNA) in the KG#471 mig-13::___ expression vector to make mig-13::tdTomato-strn-1 cDNA. Then used Q5 Polymerase to produce the fragments and the NEBuilder Master Mix to make the new plasmid.
KG#906	mig-13::__-tdTomato	Used Q5 DNA polymerase and primers engineered with restriction sites to amplify the 1.4 Kb tdTomato cDNA plasmid (gift of Dean Dawson, OMRF) and cloned it into Kpn I/ Xho I cut KG#471 (7.1 kb; mig-13::___ expression vector).
KG#917	mig-13::STRN-1--Emerald	Used Q5 polymerase and primers engineered with restriction sites to amplify the 1.4 Kb strn-1 cDNA and C-terminal linker from KG#797 unc-129::strn-1--GFP and cloned it into Not I/ Kpn I cut KG#920 (mig-13::INS-22-Emerald), removing INS-22 to leave the 7.8 Kb vector fragment).
KG#918	mig-13::SAD-1--Emerald	Used Q5 polymerase and primers engineered with restriction sites to amplify the 2.7 Kb sad-1 cDNA (adding the same C-terminal linker) from KG#695 unc-129::sad-1-GFP and cloned it into Not I/ Kpn I cut KG#920 (mig-13::INS-22-Emerald), removing INS-22 to leave the 7.8 Kb vector fragment).
KG#919	mig-13::__-tdTomato with NotI site	Used the Q5 Site-Directed Mutagenesis Kit to insert a Not I site in KG#906 plasmid. Digested with Not I to verify that the modification was successful.
KG#920	mig-13::INS-22-Emerald with Not I site	Used the Q5 Site-Directed Mutagenesis Kit to insert a Not I site in KG#859 plasmid. Digested with Not I to verify that the modification was successful.
KG#921	mig-13::SAD-1--tdTomato	Used Q5 polymerase and primers engineered with restriction sites to amplify the 2.7 Kb sad-1 cDNA (including the C-terminal linker) from KG#918 mig-13::SAD-1-Emerald and cloned it into Not I/ Kpn I cut KG#919 (mig-13::___-tdTomato; 8.1 Kb).
KP#1383	unc-129::NLP-21-Venus	Gift of Joshua Kaplan and Derek Sieburth, Massachusetts General Hospital/ Harvard University (Sieburth et al., 2007)
KS#5	odr-1::GFP	Gift of Kang Shen, Stanford University (Klassen and Shen, 2007)
pPD94.81	unc-54::GFP	Gift of Andrew Fire, Stanford University
pJP118	U6::sgRNA (F+E) (gRNA F+E plasmid)	Gift of Andrew Fire and Joshua Arribere, Stanford University

File S1. Supplemental Materials and Methods and Supplemental Material References

Growth and mounting of strains for imaging

Strain growth: Young adult progeny that had not previously been starved were grown for imaging as described (Edwards et al., 2015a). Growth times and plating numbers were modified for slow growing or lower fertility strains, such as strains containing *syd-2(ok217)* or *nud-2(ok949)*. ~55 young adults were selected and transferred to an unseeded plate immediately prior to mounting as described below.

Agarose pad slide production: Clean glass slides were produced as described (Edwards et al., 2015a). We produced ~18-19 mm diameter agarose pads, except we standardized the agarose concentration at 4% in M9 buffer as follows. After melting 0.4 g of agarose in 10 mls of M9 in a 50 ml Pyrex bottle (Thermofisher, No. 1395) with the lid screwed as tight as possible, we cooled the bottle on a folded paper towel for 2 min, slowly unscrewed the cap to prevent boiling, and poured 0.5 ml of the molten agarose into up to 10 X 1.5 ml microcentrifuge tubes in a 100° Isotemp block (Fisher) for distribution to clean slides as described, using a method described for standardizing agarose pad slides for time lapse video microscopy (Edwards et al., 2015a).

Mounting animals on agarose pad slides: For imaging lysosomes and early endosomes, we applied a 30 μl drop of 30 mg/ ml BDM (2, 3-Butanedione monoxime; Sigma B0753) in M9 buffer to a 24 X 30 mm coverslip. We then transferred the pre-picked animals into the drop in one pick-full and incubated them for 10 min, placing the coverslip on a 1.5 cm square pad of folded paper towel tissue under a Petri plate lid. For imaging synaptic vesicles or active-zone foci, we incubated animals in a 30 μl drop of 6 mM Levamisole (Sigma L9756) in M9 buffer and reduced the incubation time to 6:10 min. After the incubation, we removed ~19 μl of the solution using a P20 microinjection tip (Eppendorf 5242 956.003), leaving the worms behind in the remaining anesthetic, and inverted the coverslip onto a ~18-19 mm diameter 4% agarose pad that had been dried without its protective coverslip for the final 4 min of the incubation. We imaged animals over the next 35 – 55 min.

Image acquisition and processing

We viewed animals using a Nikon Eclipse Ti-E inverted microscope equipped with a Nikon CFI Apo TIRF 100X/ 1.49 N.A. objective, a Nikon motorized high resolution z-drive, and a motorized filter turret containing GFP, YFP, and Texas Red filter cubes (Semrock). Our illumination source was a SOLA Light Engine LED source (Lumencor). Except as indicated, we acquired images with an ORCA Flash 4.0 16-bit camera (Hamamatsu, Bridgewater, NJ) controlled by Metamorph v. 7.7. The images in Figure 9 B,C were acquired using a higher resolution ORCA AG camera. We controlled exposure times by using Metamorph to turn the LEDs on and off rather than using a shutter. We only collected images from animals with their ventral or dorsal surfaces facing the objective and “center quad” (center quadrant) mode of the camera. Z-series interval sizes (0.312 μm) and plane numbers (16) were the same for all strains and transgenes. Exposure times were identical for different strains in each experiment and chosen to collect at sub-saturating levels. Before imaging each strain, we measured the light power of the peak emission wavelength at the objective using an XR2100 power meter (Lumen Dynamics) and an XP750 objective plane light sensor (Lumen Dynamics) with the stage position set at a standard distance (z-position) from the objective. We then adjusted the percent power of the SOLA Light Engine to produce the targeted mW power for the experiment. We used AutoDeblur Gold CWF (Media Cybernetics) to deconvolve the image stacks using the Adaptive PSF blind method and 10 iterations at the low noise setting. After deconvolving, we used Metamorph to make maximum intensity projections of each image stack.

Quantitative image analysis

We used Metamorph 7.7 for most analysis and quantification. To quantify fluorescence intensities per micron, we used the Trace Region tool to trace the region and used the Multiline tool to obtain the length of the traced region. We then copied and moved the region to a similar "on animal" background region for use in background subtraction. For dorsal axons, we traced the entire axon length across the image. To trace the dendrite regions around DA6 and DB6, we used the multi-line tool to trace 20 microns along the dendrite starting at one of the cell soma boundaries that faces the other cell soma. If the region between and including the two somas was >20 μm, we deleted these lines and started each of the two dendrite regions at the outer edge of each soma, proceeding outward to each edge of the image. If the region between and including the two somas was <=20 μm, we made a 2nd line that follows the dendrite in the opposite direction starting at the inner boundary of the other cell soma and proceeding in the opposite direction. If we came to the other cell soma before reaching 20 μm, we continued measuring across the soma to the dendrite on the other side of the soma until we reached 20 μm. We then started our dendrite traces at the end of each of these two lines, proceeding outward to each edge of the image using the Trace Region tool and combining the data from the two dendrite regions. Axonal and dendritic data were logged to a spreadsheet, which subtracted the background and computed the total fluorescence per micron of length.

To quantify DA6/ DB6 cell soma intensity per square micron from maximum projected images, we traced each of the 2 somas separately and added them together, again using the traces to make "on animal" background regions for subtraction. If necessary, fluorescence from a co-injected marker expressed from the same promoter was used to identify the soma boundaries.

To quantify puncta per micron, we set a minimum pixel intensity threshold after viewing a series of images collected from *unc-16* mutant dorsal axons. We then used the Threshold plug-in of Metamorph to highlight all pixels in the region that exceeded the threshold and counted the pixel clusters that exceeded this value, irrespective of the number of pixels in the cluster. We used the same threshold value in all strains throughout the experiment.

After quantifying an image set, we produced representative images for display by saving an 8-bit version of an image that was close to mean +/- standard error for the set. All representative images within an experiment were scaled identically.

Special imaging methods

Imaging SVs in the DA9 synaptic region and soma: SVs were marked in DA9 with the SV marker GFP-RAB-3 using the *wyIs85* genomically-integrated transgenic array (Klassen and Shen, 2007). Images were collected in full-frame camera mode and processed by deconvolution as described above. To quantify the synaptic region, we used the trace region tool in Metamorph to trace the brightest 40 micron part of the synaptic region and a corresponding "on animal" background region. In ventrally oriented animals, we traced the DA9 soma and the first 20 μm of the dendrite as indicated in the Fig 4 drawing.

Quantifying invasion of uncaptured SVs into the DA9 asynaptic region: To obtain high resolution images of SVs in the entire DA9 dorsal axon (~500 microns in length), we acquired 3-4 overlapping full-frame images (designated a-d) spanning from the posterior bend of the axon through to the end of the axon (near the vulva). Images were processed by deconvolution as described above. Points of overlap between images were determined by identifying landmarks common to both images. To determine the length of the region with SVs, we first set a threshold for minimal SV cluster intensity using the wild type image set. We then applied this threshold to all strains in the experiment. We measured the length of the region from the first posterior cluster that exceeded the threshold to the last anterior cluster that exceeded the threshold. For strains with extensive invasion of uncaptured SVs into the asynaptic region, this required adding together lengths from multiple images, excluding regions of overlap between images. An Excel workbook accepted the a, b, and c lengths, added them together for total length, and then determined the mean, standard deviation, and standard error of the mean.

Profile plots of SV fluorescence in the DA9 axon: To plot the SV fluorescence distribution in DA9, we used the Plot Profile module of Image J. We used the segmented line tool with a line width of 20 pixels to trace along the length of the axon in each of 3 overlapping images comprising the DA9 axon (see above). We started at the posterior bend and ended at the end of the DA9 axon. We created profile plots from each of the 3-4 overlapping images in the set. The Y-axis maximum was set to the highest Y value in the 3 overlapping images of the set. We then copied the plot values into a SigmaPlot workbook. We saved the SigmaPlot graphs (one for each of the 3-4 overlapping images of the set) as JPEGs, imported them into Canvas and cropped them. We then used Object > Scale to shrink the vertical dimension and expand the horizontal dimension. The 3 graphs were further cropped and merged together at their points of overlap to make a single high resolution profile plot comprising the entire DA9 dorsal axon.

High resolution sub-bouton images of Sentryn-emerald: We used an ORCA AG camera on the above microscope system. The ORCA AG has a significantly smaller pixel size than the Flash 4.0 camera and thus allows higher resolution images. We collected stacks of 10 images separated in the z-plane by 0.14 microns each. In addition, the image stacks were resized by a factor of 2 in the X and Y planes prior to deconvolution using the “Ideal” algorithm in Autodeblur Gold CWF to maintain quantitative accuracy. In so doing, each pixel size was reduced to 32.25 nm X 32.25 nm to maximize resolution to the diffraction limited level.

Immunostaining of formaldehyde-fixed animals

Freeze cracking and fixing animals: We prepared freeze-cracked 4% paraformaldehyde fixed, young adult worms for immunostaining as described (Charlie et al., 2006a; Charlie et al., 2006b), with the exception that we modified the freeze cracking procedure as follows to prevent the fixative from freezing during freeze cracking. Steps before and after freeze cracking were identical to the above published procedures. To freeze crack worms, we filled one 50 ml conical per strain with 40 mls of 4% formaldehyde in 1X PBS, pH 7.4. The fixative was made fresh by breaking a 10 ml ampule of 16% formaldhyde (Ted Pella EM grade #NC9658705) and mixing its contents with 26 mls of ddH2O and 4 mls of 10X PBS in a 50 ml conical. The 50 ml conical with fixative was immersed in ice for at least 45 min. Freshly frozen slide sandwiches containing ~1500 young and mature adults sandwiched between two overlapping glass slides were prepared as described (Charlie et al., 2006a; Charlie et al., 2006b). Then, up to 12 such sandwiches were successively cracked and combined with cold fixative as follows. At time 0 sec, a count-up timer was started. The first slide sandwich was removed from its dry ice block, and the two slides of the first sandwich were vigorously separated and laid, worm-side-up on a Styrofoam surface at room temperature for 1:30 min. At 1:20 – 1:30 min, the second slide sandwich was cracked and laid next to the first two halves on the Styrofoam surface. From 1:30 min – 2:45 min, the two halves of the first sandwich were placed back-to-back and immersed in the ice cold fixative in the 50 ml conical tube, using forceps to hold the slides. The worms were rinsed off of both slides forcefully using a P1000 pipet, and then the rinsed slides were discarded. The third sandwich was then cracked at 2:50 – 3:00 min, followed by rinsing worms from the second sandwich at 3:00 – 4:15, etc. until all the worms from 2 – 12 sandwiches have been rinsed into the cold fixative. The worms were then concentrated by pouring ~1/3rd of the suspension into a 15 ml conical, spinning 2000 rpm for 10 sec in a swinging bucket rotor in a Dynac clinical centrifuge at room temperature with the brake applied, removing the supernatant with vacuum suction, and repeating twice more. We left ~ 1 ml after the 3rd spin, and then used a Pasteur Pipet or P1000 to forcefully rinse off any animals stuck to the bottom of the tube and transfer the suspension into a 1.5 ml snap-cap tube. We then spun this tube at 6000 rpm for 12 sec in a microfuge, removed most of the cold fixative, and replaced it with 1 ml of previously reserved room temperature fixative. All subsequent steps (30 min fixation at room temperature, quenching in 1 ml of 0.1M glycine, pH 7.4 for 5 min, washing with Antibody Buffer B, blocking with 3% BSA block, and staining with primary and secondary antibodies, and post-staining washes) were performed as described (Charlie et al., 2006a; Charlie et al., 2006b). For immunostaining of UNC-17-labeled SVs, we used Mouse anti-UNC-17

(1/5000 from monoclonal ascites fluid (Duerr et al., 2001). The secondary antibody was Goat anti-Mouse Dylight 550 (Pierce). We used a Semrock Cy3 filter set to view the Dylight 550 signal.

Supplementary References.

Ackley, B.D., Harrington, R.J., Hudson, M.L., Williams, L., Kenyon, C.J., Chisholm, A.D., and Jin, Y. (2005). The two isoforms of the Caenorhabditis elegans leukocyte-common antigen related receptor tyrosine phosphatase PTP-3 function independently in axon guidance and synapse formation. J Neurosci *25*, 7517-7528.

Charlie, N.K., Schade, M.A., Thomure, A.M., and Miller, K.G. (2006a). Presynaptic UNC-31 (CAPS) is required to activate the G alpha(s) pathway of the Caenorhabditis elegans synaptic signaling network. Genetics *172*, 943-961.

Charlie, N.K., Thomure, A.M., Schade, M.A., and Miller, K.G. (2006b). The Dunce cAMP phosphodiesterase PDE-4 negatively regulates G alpha(s)-dependent and G alpha(s)-independent cAMP pools in the Caenorhabditis elegans synaptic signaling network. Genetics *173*, 111-130.

Dai, Y., Taru, H., Deken, S.L., Grill, B., Ackley, B., Nonet, M.L., and Jin, Y. (2006). SYD-2 Liprin-alpha organizes presynaptic active zone formation through ELKS. Nat Neurosci *9*, 1479-1487.

Deken, S.L., Vincent, R., Hadwiger, G., Liu, Q., Wang, Z.W., and Nonet, M.L. (2005). Redundant localization mechanisms of RIM and ELKS in Caenorhabditis elegans. J Neurosci *25*, 5975-5983.

Duerr, J.S., Gaskin, J., and Rand, J.B. (2001). Identified neurons in *C. elegans* coexpress vesicular transporters for acetylcholine and monoamines. Am J Physiol Cell Physiol *280*, C1616-1622.

Edwards, S.L., Charlie, N.K., Richmond, J.E., Hegermann, J., Eimer, S., and Miller, K.G. (2009). Impaired dense core vesicle maturation in Caenorhabditis elegans mutants lacking Rab2. J Cell Biol *186*, 881-895.

Edwards, S.L., Morrison, L.M., Yorks, R.M., Hoover, C.M., Boominathan, S., and Miller, K.G. (2015a). UNC-16 (JIP3) Acts Through Synapse-Assembly Proteins to Inhibit the Active Transport of Cell Soma Organelles to Caenorhabditis elegans Motor Neuron Axons. Genetics *201*, 117-141.

Edwards, S.L., Yorks, R.M., Morrison, L.M., Hoover, C.M., and Miller, K.G. (2015b). Synapse-Assembly Proteins Maintain Synaptic Vesicle Cluster Stability and Regulate Synaptic Vesicle Transport in Caenorhabditis elegans. Genetics *201*, 91-116.

Edwards, S.L., Yu, S.C., Hoover, C.M., Phillips, B.C., Richmond, J.E., and Miller, K.G. (2013). An organelle gatekeeper function for Caenorhabditis elegans UNC-16 (JIP3) at the axon initial segment. Genetics *194*, 143-161.

Ferguson, E.L., and Horvitz, H.R. (1985). Identification and characterization of 22 genes that affect the vulval cell lineages of the nematode Caenorhabditis elegans. Genetics *110*, 17-72.

Fridolfsson, H.N., Ly, N., Meyerzon, M., and Starr, D.A. (2010). UNC-83 coordinates kinesin-1 and dynein activities at the nuclear envelope during nuclear migration. Dev Biol *338*, 237-250.

Hoover, C.M., Edwards, S.L., Yu, S.C., Kittelmann, M., Richmond, J.E., Eimer, S., Yorks, R.M., and Miller, K.G. (2014). A Novel CaM Kinase II Pathway Controls the Location of Neuropeptide Release from Caenorhabditis elegans Motor Neurons. Genetics *196*, 745-765.

Kim, S., Ko, J., Shin, H., Lee, J.R., Lim, C., Han, J.H., Altrock, W.D., Garner, C.C., Gundelfinger, E.D., Premont, R.T.*, et al.* (2003). The GIT family of proteins forms multimers and associates with the presynaptic cytomatrix protein Piccolo. J Biol Chem *278*, 6291-6300.

Kittel, R.J., Wichmann, C., Rasse, T.M., Fouquet, W., Schmidt, M., Schmid, A., Wagh, D.A., Pawlu, C., Kellner, R.R., Willig, K.I.*, et al.* (2006). Bruchpilot promotes active zone assembly, Ca2+ channel clustering, and vesicle release. Science *312*, 1051-1054.

Kittelmann, M., Hegermann, J., Goncharov, A., Taru, H., Ellisman, M.H., Richmond, J.E., Jin, Y., and Eimer, S. (2013). Liprin-alpha/SYD-2 determines the size of dense projections in presynaptic active zones in C. elegans. J Cell Biol *203*, 849-863.

Klassen, M.P., and Shen, K. (2007). Wnt signaling positions neuromuscular connectivity by inhibiting synapse formation in *C. elegans*. Cell *130*, 704-716.

Ko, J., Kim, S., Valtschanoff, J.G., Shin, H., Lee, J.R., Sheng, M., Premont, R.T., Weinberg, R.J., and Kim, E. (2003a). Interaction between liprin-alpha and GIT1 is required for AMPA receptor targeting. J Neurosci *23*, 1667-1677.
Ko, J., Na, M., Kim, S., Lee, J.R., and Kim, E. (2003b). Interaction of the ERC family of RIM-binding proteins with the liprin-alpha family of multidomain proteins. J Biol Chem *278*, 42377-42385.
Kohn, R.E., Duerr, J.S., McManus, J., Duke, A., Rakow, T.L., Maruyama, H., Moulder, G., Maruyama, I.N., Barstead, R.J., and Rand, J.B. (2000). Expression of multiple UNC-13 proteins in the *Caenorhabditis elegans* nervous system. Mol Biol Cell *11*, 3441-3452.
Koushika, S.P., Richmond, J.E., Hadwiger, G., Weimer, R.M., Jorgensen, E.M., and Nonet, M.L. (2001). A post-docking role for active zone protein Rim. Nat Neurosci *4*, 997-1005.
Liu, K.S., Siebert, M., Mertel, S., Knoche, E., Wegener, S., Wichmann, C., Matkovic, T., Muhammad, K., Depner, H., Mettke, C.*, et al.* (2011). RIM-binding protein, a central part of the active zone, is essential for neurotransmitter release. Science *334*, 1565-1569.
Ohtsuka, T., Takao-Rikitsu, E., Inoue, E., Inoue, M., Takeuchi, M., Matsubara, K., Deguchi-Tawarada, M., Satoh, K., Morimoto, K., Nakanishi, H.*, et al.* (2002). Cast: a novel protein of the cytomatrix at the active zone of synapses that forms a ternary complex with RIM1 and munc13-1. J Cell Biol *158*, 577-590.
Olsen, O., Moore, K.A., Fukata, M., Kazuta, T., Trinidad, J.C., Kauer, F.W., Streuli, M., Misawa, H., Burlingame, A.L., Nicoll, R.A.*, et al.* (2005). Neurotransmitter release regulated by a MALS-liprin-alpha presynaptic complex. J Cell Biol *170*, 1127-1134.
Patel, M.R., Lehrman, E.K., Poon, V.Y., Crump, J.G., Zhen, M., Bargmann, C.I., and Shen, K. (2006). Hierarchical assembly of presynaptic components in defined C. elegans synapses. Nat Neurosci *9*, 1488-1498.
Schoch, S., Castillo, P.E., Jo, T., Mukherjee, K., Geppert, M., Wang, Y., Schmitz, F., Malenka, R.C., and Sudhof, T.C. (2002). RIM1alpha forms a protein scaffold for regulating neurotransmitter release at the active zone. Nature *415*, 321-326.
Serra-Pages, C., Medley, Q.G., Tang, M., Hart, A., and Streuli, M. (1998). Liprins, a family of LAR transmembrane protein-tyrosine phosphatase-interacting proteins. J Biol Chem *273*, 15611-15620.
Sieburth, D., Madison, J.M., and Kaplan, J.M. (2007). PKC-1 regulates secretion of neuropeptides. Nat Neurosci *10*, 49-57.
Wagh, D.A., Rasse, T.M., Asan, E., Hofbauer, A., Schwenkert, I., Durrbeck, H., Buchner, S., Dabauvalle, M.C., Schmidt, M., Qin, G.*, et al.* (2006). Bruchpilot, a protein with homology to ELKS/CAST, is required for structural integrity and function of synaptic active zones in Drosophila. Neuron *49*, 833-844.
Wagner, O.I., Esposito, A., Kohler, B., Chen, C.W., Shen, C.P., Wu, G.H., Butkevich, E., Mandalapu, S., Wenzel, D., Wouters, F.S.*, et al.* (2009). Synaptic scaffolding protein SYD-2 clusters and activates kinesin-3 UNC-104 in C. elegans. Proc Natl Acad Sci U S A *106*, 19605-19610.
Wang, Y., Liu, X., Biederer, T., and Sudhof, T.C. (2002). A family of RIM-binding proteins regulated by alternative splicing: Implications for the genesis of synaptic active zones. Proc Natl Acad Sci U S A *99*, 14464-14469.
Wang, Y., Okamoto, M., Schmitz, F., Hofmann, K., and Sudhof, T.C. (1997). Rim is a putative Rab3 effector in regulating synaptic-vesicle fusion. Nature *388*, 593-598.
Wang, Y., Sugita, S., and Sudhof, T.C. (2000). The RIM/NIM family of neuronal C2 domain proteins. Interactions with Rab3 and a new class of Src homology 3 domain proteins. J Biol Chem *275*, 20033-20044.
Weimer, R.M., Gracheva, E.O., Meyrignac, O., Miller, K.G., Richmond, J.E., and Bessereau, J.L. (2006). UNC-13 and UNC-10/rim localize synaptic vesicles to specific membrane domains. J Neurosci *26*, 8040-8047.